



Contents lists available at ScienceDirect

## Materials Today: Proceedings

journal homepage: [www.elsevier.com/locate/matpr](http://www.elsevier.com/locate/matpr)

# Low temperature synthesis and influence of rare earth Nd<sup>3+</sup> substitution on the structural, magnetic behaviour of M-type barium hexa ferrite nanomaterials

Harendra Kumar Satyapal, Rakesh Kumar Singh\*, Nishant Kumar, Saurabh Sharma

Aryabhata Centre for Nanoscience and Nanotechnology, School of Engineering and Technology, Aryabhata Knowledge University, Patna 800001, India

## ARTICLE INFO

## Article history:

Received 24 January 2020

Received in revised form 29 January 2020

Accepted 31 January 2020

Available online xxx

## Keywords:

M type-hexa ferrite

Sol-gel method

Nd<sup>3+</sup> substitution

Microstructure

Curie temperature

## ABSTRACT

The (Nd<sup>3+</sup>) substituted M-type Barium hexaferrite (BaFe<sub>12-x</sub>Nd<sub>x</sub>O<sub>19</sub>) with (Nd<sup>3+</sup>) concentration ( $x = 0, 0.25, 0.50, 0.75, 1.00$ ) is prepared using citrate precursor based sol gel process. The X-ray intensity pattern confirms that synthesized nanomaterials were in the pure phase and they possess hexagonal crystal structure having  $P6_3/mmc$  space group. Crystallite size and lattice strain values decreased with increment in concentration of Nd<sup>3+</sup> in Barium Hexaferrite lattice. The Williamson-Hall plot is utilized for calculating these structural parameters. The Saturation Magnetization and Anisotropy values are highest for (0.25) mole (Nd<sup>3+</sup>) in Barium Hexaferrite lattice. All the prepared nanomaterials shows pure phase with good magnetization (43.11 emu/g–56.90 emu/g), retentivity (21.41 emu/g–29.02 emu/g) at room temperature. Curie temperature was found to be shifted to 429 °C from 446 °C with respect to increasing molar concentration of Neodymium.

© 2020 Elsevier Ltd. All rights reserved.

Selection and Peer-review under responsibility of the scientific committee of the International Conference on Advanced Materials and Nanotechnology.

## 1. Introduction

Ferrite nanomaterials possess high commercial value due to its significant magnetic properties along with its prominent uses in electronics industries, as radar absorbing, in high frequency power applications, hydroelectric cell, information storage etc. [1–5]. Ferrite materials have been classified into 3 categories: Spinel, Garnet and Hexaferrite. The industrial demands for hexaferrite nanomaterials is more due to suitability of hexaferrite as high density recording media and microwave absorption properties. Based on chemical nature and unit cell structure Hexa ferrite are subdivided into five sections. M-type (BaFe<sub>12</sub>O<sub>19</sub>), W-Type (BaT<sub>2</sub>Fe<sub>12</sub>O<sub>27</sub>), X-Type (Ba<sub>2</sub>T<sub>2</sub>Fe<sub>28</sub>O<sub>46</sub>), Y-Type (Ba<sub>2</sub>T<sub>2</sub>Fe<sub>12</sub>O<sub>22</sub>) and Z-type (Ba<sub>3</sub>T<sub>2</sub>Fe<sub>24</sub>O<sub>41</sub>). Where 'T' stands for any divalentions, trivalent ions or tetravalent metal ions [6]. The M-type Barium hexaferrite (BaFe<sub>12</sub>O<sub>19</sub>) possess magneto plumbite structure with hexagonal crystal system and have ( $P6_3/mmc$ ) space group. Barium hexaferrite lattices have c-axis to be the magnetically preferred axis. There ported Coercivity and magnetization values for such hexaferrite materials are 6700 Oe and 72 emu/g respectively and its curie point is 450 °C, which is

quite above the room temperature [7]. Therefore such exceptional behaviours make hexaferrite material to gain widespread attention of researchers in recent years [8–11]. The crystal structure of (BaFe<sub>12</sub>O<sub>19</sub>) have S block and R block superimposed. Its unit cell have the order RSR\*S\*. Here S\* and R\* possess same atomic arrangements but they are 180° rotated with reference to S and R blocks [12–14]. The magnetic behaviour of BaFe<sub>12</sub>O<sub>19</sub> is dependent on the placement of Fe<sup>3+</sup> ions in the crystal geometry, annealing temperature, substituted element and method of preparation [15–17]. Numerous researchers have mentioned about enhanced physical characteristics of BaFe<sub>12</sub>O<sub>19</sub> by manipulating the cation distribution of different ionic radii such as with Sm<sup>3+</sup>, Mn<sup>3+</sup>, Ce<sup>2+</sup>, Ni<sup>2+</sup>, Al<sup>3+</sup> etc. [18–29]. The detailed literature works reveals that researchers are concentrating upon the cation placement on atomic sites and consequent alterations on magnetic behavior. Along with cation distribution, the developed lattice strains are found to be affecting magnetic properties. Therefore the crystal structural effects and its correlation with room temperature magnetism and Curie temperature dependent magnetic responses for (BaFe<sub>12-x</sub>Nd<sub>x</sub>O<sub>19</sub>) with Neodymium varying concentration has been explored in the present research. The magnetic nanomaterials were prepared using low cost chemical based citrate precursor method in low temperature range of 200°Celsius, which is economical and convenient for mass production for

\* Corresponding author.

E-mail address: [rakeshsinghpu@gmail.com](mailto:rakeshsinghpu@gmail.com) (R. Kumar Singh).

numerous uses. To the best of our knowledge very few research works have been reported on  $\text{Nd}^{3+}$  substituted M-type Barium hexa ferrite nanomaterials.

## 2. Experimental details

The pure phase Barium Hexaferrite ( $\text{BaFe}_{12}\text{O}_{19}$ ) and four different molar concentration of  $\text{Nd}^{3+}$  substituted  $\text{BaFe}_{12}\text{O}_{19}$  (BHF) was prepared using low cost chemical based citrate precursor sol-gel method. Chemicals used were of high purity grade namely,  $\text{Ba}(\text{NO}_3)_2$ ,  $\text{Nd}(\text{NO}_3)_3$ , and  $\text{Fe}(\text{NO}_3)_3$ . For chelation in the synthesis procedure, citric acid was used. The stoichiometric ratio of citric acid to metal cations were kept to be 1:3. After stirring the mixture containing stoichiometric ratio of chemical nitrates in deionized water on hot plate for 3–4 h, a gel like substance is obtained. Which was then kept in hot air oven throughout the night to dry. Finally a voluminous like ash powder is obtained, further grinded to fine powder with Mortar and Pestle. The powdered nanomaterial was further put for annealing at  $800^\circ\text{C}$  for 2hr. The room temperature X ray diffraction pattern were obtained at wavelength ( $\lambda = 1.5406 \text{ \AA}$ ) using Bruker D8 advance X ray Diffractometer. Magnetic hysteresis loop (M-H) loops and Curie points (M-T) graphs were calculated at room temperature using Lakeshore(7500,USA) vibrating sample magnetometer capable with magnetic field upto (3.2 Tesla). The arrangement of particles and surface morphology of the samples were examined with FESEM (Carl Zeiss) and functional group were found using Fourier Transform infrared spectroscopy (FTIR, Perkin Elmer).

## 3. Results and discussion

**Structural properties-** X ray diiffraction peaks confirmed that synthesized nanomaterials were in pure phase and all possess hexagonal crystal structure and belongs to space group  $P6_3/mmc$  are shown in Fig. 1. X ray intensity peaks are in agreement to that of earlier reports [30]. There is a gradual shifting in the XRD peaks towards a greater Bragg's angle with the increment in molar concentration of Neodymium in Barium hexaferrite. It can be observed precisely that (107) peak shifts from (32.12) degree for ( $\text{BaFe}_{12}\text{O}_{19}$ ) to (32.23) degree for ( $\text{BaFe}_{12-x}\text{Nd}_x\text{O}_{19}$ ) as shown in Fig. 2. Such observation may be due to bigger ionic radius of  $\text{Nd}^{3+}$  (1.12  $\text{\AA}$ ) with respect to  $\text{Fe}^{3+}$  ions (0.64  $\text{\AA}$ ).

Further substitution of neodymium at iron site results into systematic increment of lattice parameter(c) only and so increment in

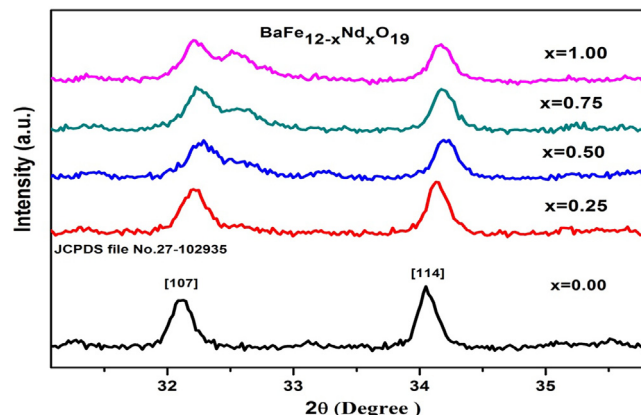


Fig. 2. Peak shift for planes [107] and [211] towards higher Bragg's angle.

cell volume (Table 1). The lattice parameters(a) is almost constant. The crystalline size and strains in nanomaterial were obtained by Williamson-Hall method. The Williamson-Hall relation is defined as [31]

$$B\cos\theta = K\lambda + 4\epsilon\sin\theta \quad (1)$$

In the above Eq. (1)  $\lambda$  denotes x-ray wavelength incident on samples,  $\theta$  is the Bragg's diffraction angle. Further D is used for crystalline size and  $\beta$  is full width at half the intensity maximum plotted versus  $2\theta$  Bragg's angle. The term ( $4\epsilon \sin \theta$ ) is strain and intercept ( $K\lambda/D$ ) on the ordinate ( $B\cos\theta$ ) helps to find the crystalline size. The W-H plots for XRD patterns of ( $\text{BaFe}_{12-x}\text{Nd}_x\text{O}_{19}$ ) for  $x = 0.0$  to 1.0 are shown in Fig. 3(a-e). The plots are lineally fitted. Intercepts on the y axis is helpful in finding the value of crystallite size while inclination of the straight line gives amount of lattice strain present. Both crystallite size and strains in the lattices are mentioned in the Table 1. It is clearly observed that there is decrement of lattice strain with the increment in the Neodymium concentration. Larger atomic radius of  $\text{Nd}^{3+}$  ions as compared to  $\text{Fe}^{3+}$  ions may be one of the reason. The crystallite size obtained using W-H plot may differ from that of the particle size [31].

Therefore surface morphology in FESEM micrographs are utilized for justifying the crystallite size obtained using W-H plots. As such a high resolution micrograph of ( $\text{BaFe}_{11.25}\text{Nd}_{0.75}\text{O}_{19}$ ) is also shown in Fig. 4(a-b). Particles are visible to be uniformly distributed. Surface area and crystalline size are linked to each other. As the crystallite size decreases systematically, there is increment in the number of atoms appearing at the surface. Agglomerated nanocrystalline materials can be seen in Fig. 4. Lattice constants for this very hexagonal crystal system is calculated using Eq. (2). Planes which were utilized in this equation are [110],[107],[114], [217],[220] and [2011]. Once the lattice constants are determined, we can easily calculate the lattice volume for this crystal system using Eq. (3). There is a increment in the lattice constants(c) and lattice volume. Presence of  $\alpha\text{-Fe}_2\text{O}_3$  in the synthesized sample may be a probable reason but the intensity of this peak is very small. Such observances have been also reported by Ping Xu et al. research groups [32]. Crystalline size was found to decrease systematically instead of increases with increase in molar concentration of Nd. This may be because of systematic decrement of strain in the prepared materials.

$$\frac{1}{d^2} = \frac{4}{3} \left( \frac{h^2 + hk + k^2}{a^2} \right) + \frac{l^2}{c^2} \quad (2)$$

$$V = \frac{(3)1/2}{2} a^2 c \quad (3)$$

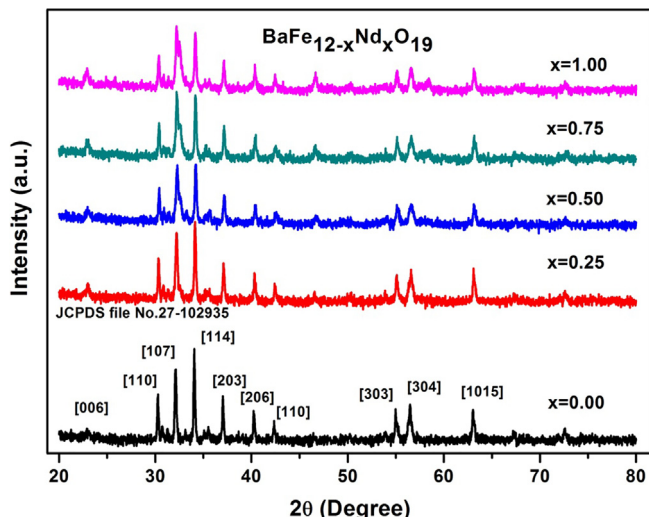
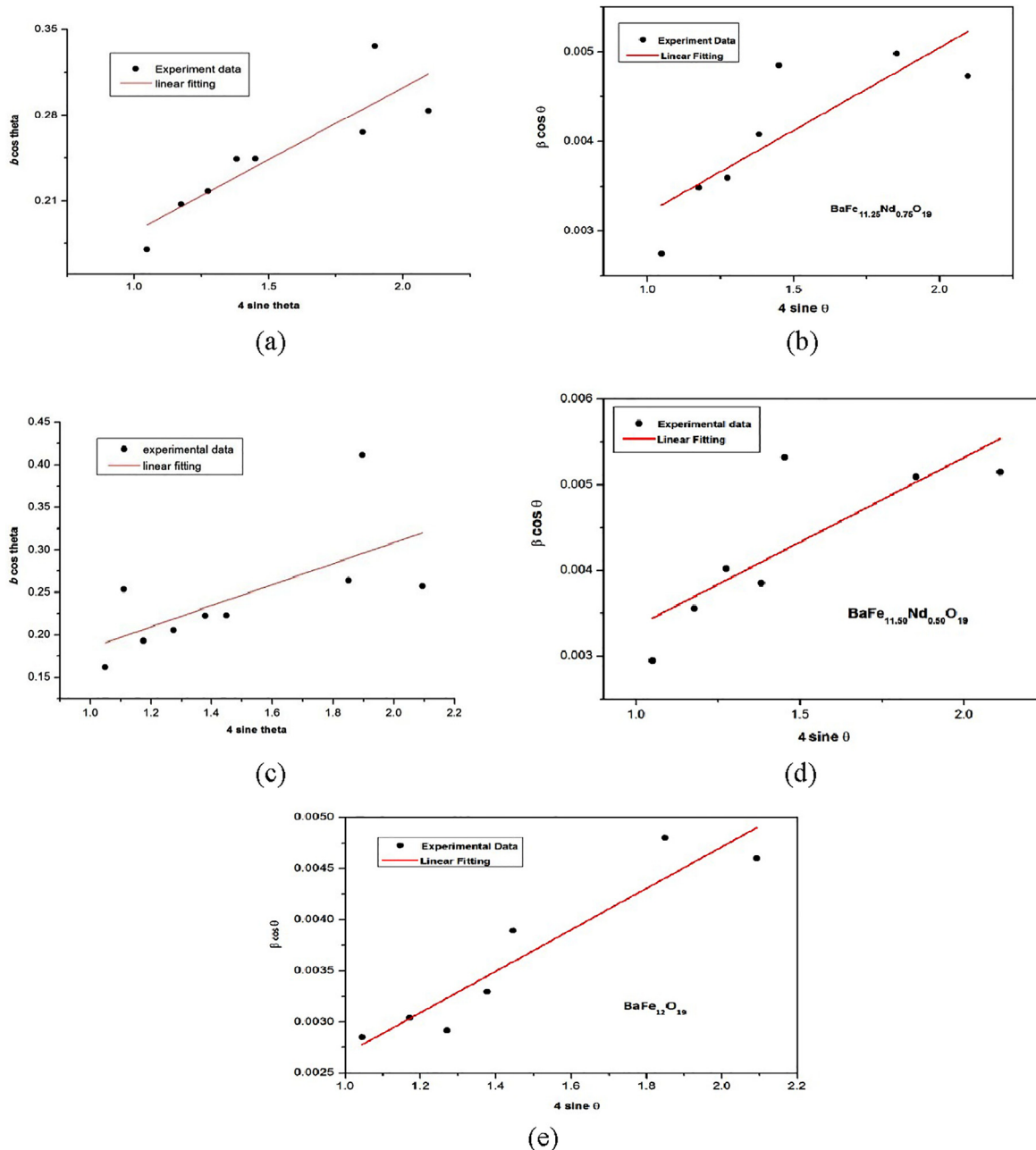


Fig. 1. X ray spectrum of BHF ( $\text{BaFe}_{12-x}\text{Nd}_x\text{O}_{19}$ ) for  $x = 0.0$  to 1.0).

**Table 1**  
Structural parameters details of crystallite size and Lattice strain.

Samples BaFe <sub>12-x</sub> Nd <sub>x</sub> O <sub>19</sub>	Crystallite size (Williamson Hall) nm (-+Error)	Strain × 10 <sup>-3</sup>	Crystal structure details		
			a = b(Å)	c(Å)	cell volume (Å <sup>3</sup> )
x = 0	82.9 (-+1)	2.03	5.8847	23.15	694.252
x = 0.25	76.2 (-+1)	1.97	5.8878	23.18	695.884
x = 0.50	74.6 (-+1)	1.85	5.8921	23.20	697.503
x = 0.75	67.1 (-+1)	1.67	5.8947	23.21	698.419
x = 1.00	64.9 (-+1)	1.54	5.8981	23.23	699.828



**Fig. 3.** W-H plots for  $(\beta \cos \theta)$  versus  $(4 \sin \theta)$  to estimate crystallite size and lattice strain. (a) BaFe<sub>11</sub>Nd<sub>1</sub>O<sub>19</sub> (b) BaFe<sub>11.25</sub>Nd<sub>0.75</sub>O<sub>19</sub> (c) BaFe<sub>11.50</sub>Nd<sub>0.50</sub>O<sub>19</sub> (d) BaFe<sub>11.75</sub>Nd<sub>0.25</sub>O<sub>19</sub> (e) BaFe<sub>12</sub>O<sub>19</sub>.

### 3.1. FTIR measurements

The FTIR absorption spectra for (BaFe<sub>12-x</sub>Nd<sub>x</sub>O<sub>19</sub>) is shown in Fig. 5, For (x = 0.25 to 1) at room temperature with wave number (400 cm<sup>-1</sup>–700 cm<sup>-1</sup>). For Barium hexaferrite, two prominent IR modes are noticed at (439 cm<sup>-1</sup>) and (602 cm<sup>-1</sup>) for bonds at the

octahedral sites and tetrahedral sites respectively [33]. The frequency limit (439–459) cm<sup>-1</sup>, peak ( $\nu_1$ ) is helpful in finding octahedral bond length.

The lighter frequency range (602–616) cm<sup>-1</sup>, peak ( $\nu_2$ ) is useful in finding tetrahedral bond length of (Fe-O) and (Nd-O) [33]. The vibrational frequency of tetrahedral is greater than octahedral

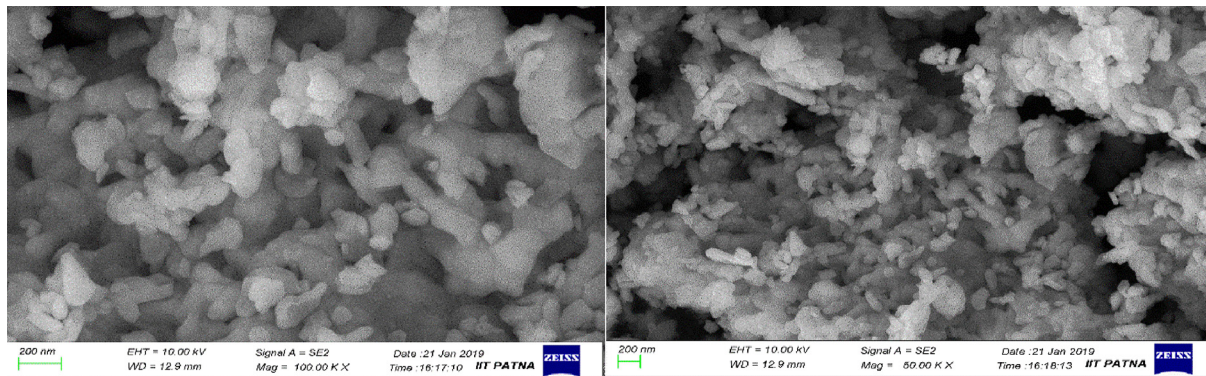


Fig. 4. FESEM micrograph for  $(\text{BaFe}_{12-x}\text{Nd}_x\text{O}_{19})$  for  $x = 0.75$  samples.

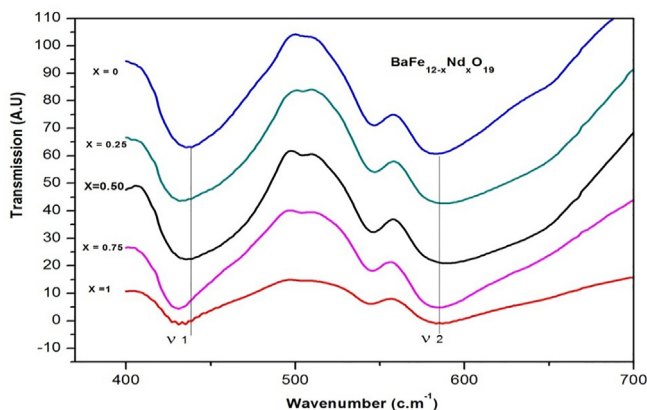


Fig. 5. FTIR spectrum for Barium hexaferrite doped with Neodymium  $(\text{BaFe}_{12-x}\text{Nd}_x\text{O}_{19})$ .

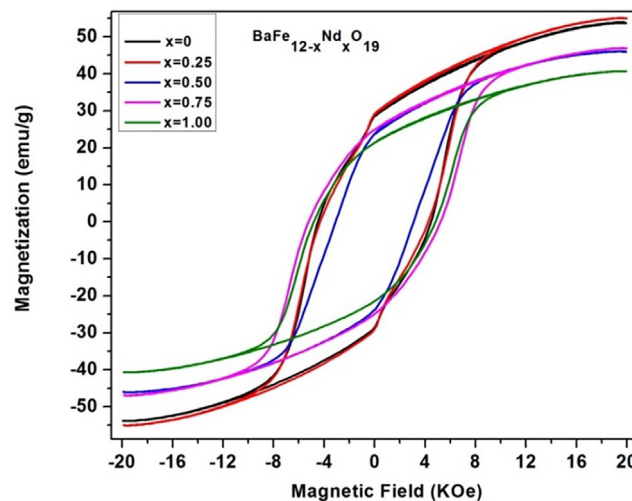


Fig. 6. MH loops for  $(\text{BaFe}_{12-x}\text{Nd}_x\text{O}_{19})$  with  $(x = 0 \text{ to } 1.0)$  at room temperature.

due to larger bond length of octahedral sites. The absorption peak shifts towards the lower wavenumber due to substitution of bigger neodymium ions in place of iron atoms. Such observations has been also mentioned by other reseachers [34].

### 3.2. Magnetic properties

Magnetic Hysteresis loop for neodymium substituted BHF  $(\text{BaFe}_{12-x}\text{Nd}_x\text{O}_{19})$  for  $(x = 0.0-1.0)$  is depicted in Fig. 6. Magnetisation curves showing ferromagnetic behavior, high coercive field values are found. It appears that it has not achieved saturation at 2 Tesla. The coercivity  $(H_c)$ , Magnetization values  $(M_s)$ , Retentivity  $(M_r)$ , anisotropic constant and magnetization vs  $1/H^2(\text{Oe})^2$  plot have been enlisted in Table 2 and Fig. 7.

The remanant magnetization and saturation magnetization both magnetic parameters first increases and then decreases with increment in neodymium amount. The Coercivity value are highest for 0.75 mol Nd doped Barium hexaferrite and with increment in Nd concentration Coercivity values decreases irregularly. This reveal about formation of single domain particles with uniaxial anisotropy. It may be due to lattice strain developed with the neodymium doping at iron site. The saturation magnetization is calculated with help of Law of approach.

This is fruitful in finding out two useful parameters, first one Magnetization  $(M_s)$  and second one, Anisotropy constant denoted by  $(K_1)$  such nanomaterials [35]. The magnetization value and magneto crystalline anisotropy values are highest for 0.25 mol Neodymium doped Barium hexaferrite. The law of approach is expressed as [36].

$$M = M_s \left[ 1 - \left( \frac{A}{H} \right) - \left( \frac{B}{H^2} \right) \right] + \chi H \quad (4)$$

Here  $M_s$  is for magnetization, and  $A$  is a material constant  $B$  is magneto crystalline anisotropy field. Further  $\chi H$  is high field differential susceptibility countable in high temperature analysis only [33]. Also  $A/H$  is not a significant value. Finally Eq. (4) reduces as

$$M = M_s \left[ 1 - \left( \frac{B}{H^2} \right) \right] \quad (5)$$

The anisotropy is expressed as equation [34]

$$B = H_a^2 / 15 \quad (6)$$

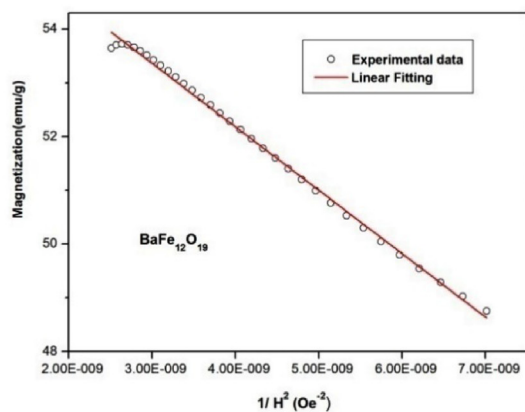
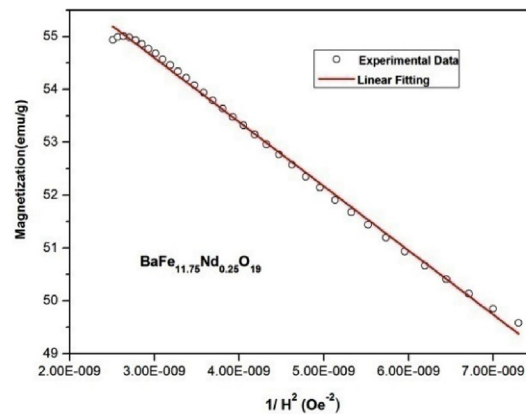
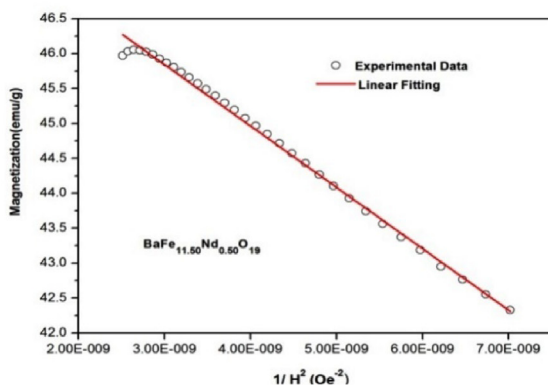
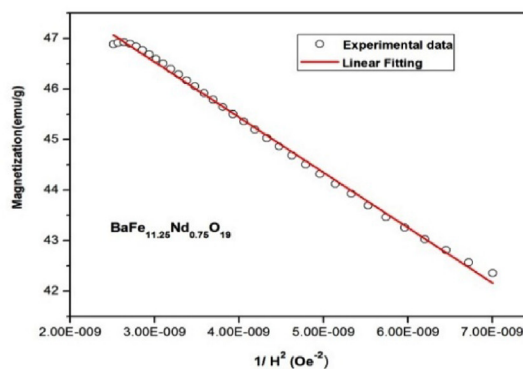
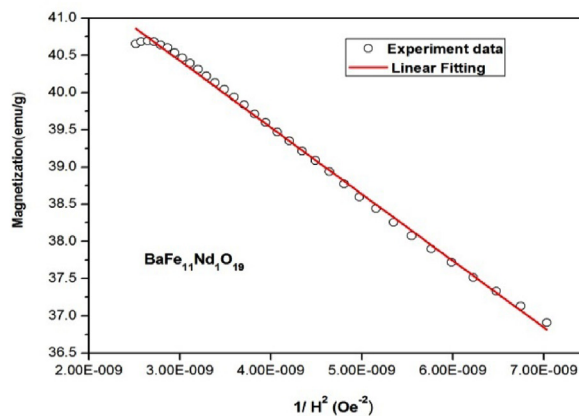
The magneto anisotropy is calculated using expression

$$H_a = (2K_1) / M_s \quad (7)$$

The intercept on the ordinate of the linearly fitted curve of the Magnetization versus  $(1/H^2)$  plot helps us to determine the value of magnetization  $(M_s)$  which is shown in Fig 7(a) to 7(e). The amount of magneto anisotropy field  $B_1$  can be found from the slope of linearly fitted curve. Further Eqs. (6) and (7) is utilized for finding out magneto crystalline anisotropy  $(K_1)$  value. All the concerned magnetic parameters are mentioned in Table 2. As shown in Table 2, Saturation magnetization as well as Magneto anisotropy constant value is greatest for  $(\text{BaFe}_{11.75}\text{Nd}_{0.25}\text{O}_{19})$ . Therefore there is a continual decrement in both these magnetic parameters  $(M_s$  and  $K_1)$  for higher molar concentration of neodymium in Barium hexaferrite lattice. It may be because, change in super exchange interaction of

**Table 2**Magnetic property details of  $(\text{BaFe}_{12-x}\text{Nd}_x\text{O}_{19})$  with  $(x = 0 \text{ to } 1.0)$ .

Molar ratio	Magnetic properties				
$\text{BaFe}_{12-x}\text{Nd}_x\text{O}_{19}$	Magnetization (Ms) (emu/g)	Retentivity (Mr) (emu/g)	Coercivity $H_c$ (Oe)	Anisotropy field $B 10^8(\text{Oe}^2)$	Anisotropic constant $K_1 (10^6 \text{ erg/cm}^3)$
$x = 0.00$	56.90	28.54	4477.9	11.8	3.78
$x = 0.25$	58.24	29.02	4289.5	12.1	3.92
$x = 0.50$	48.47	23.70	3086.1	8.78	2.78
$x = 0.75$	49.81	24.86	5234.4	10.9	3.18
$x = 1.00$	43.11	21.41	4819.1	8.95	2.49

(a). Moment vs  $(1/H^2)$  plot for  $\text{BaFe}_{12}\text{O}_{19}$ (b). Moment vs  $(1/H^2)$  plot for  $(\text{BaFe}_{11.75}\text{Nd}_{0.25}\text{O}_{19})$ (c). Moment vs  $1/H^2$  plot for  $(\text{BaFe}_{11.50}\text{Nd}_{0.50}\text{O}_{19})$ (d). Moment vs  $(1/H^2)$  plot for  $(\text{BaFe}_{11.25}\text{Nd}_{0.75}\text{O}_{19})$ (e). Moment vs  $1/H^2$  plot for  $(\text{BaFe}_{11}\text{Nd}_1\text{O}_{19})$ **Fig. 7.** (a-e) Magnetization versus  $1/H^2$  plot of  $\text{BaFe}_{12-x}\text{Nd}_x\text{O}_{19}$  (for  $x = 0$  to 1 mol).

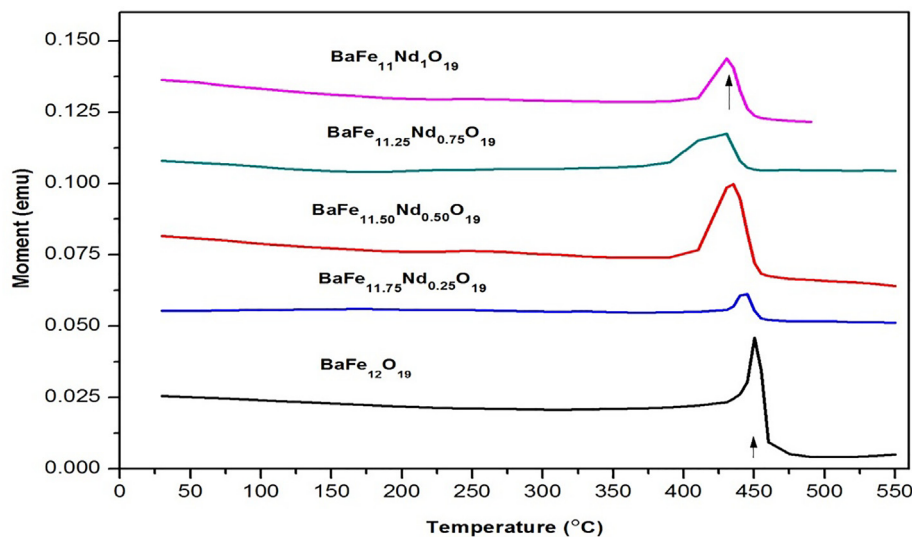


Fig. 8. Curie point measurement for sample  $(\text{BaFe}_{12-x}\text{Nd}_x\text{O}_{19})$ .

Fe-O-Fe in all concerned crystal directions [34].  $M_s$  ranges from (58.24 emu/g) to (43.11) emu/g, whereas  $K_1$  is ranging between  $(3.92 \text{ and } 2.49) \times 10^6 \text{ erg/cm}^3$ . This may be because of lesser magnetic moment value ( $3\mu_B$ ) of Nd ion with respect to  $\text{Fe}^{3+}$  ion ( $5\mu_B$ ). Such behavior is in agreement with work reported by research groups [37]. Lattice strain shows regular decrement in its value with the increase in the neodymium concentration. The strain reaches to a minimal value ( $1.54 \times 10^{-3}$ ) for 1 mol neodymium concentration. It may be due to greater ionic radii of neodymium with respect to iron ions radii. As also observed by research groups [38]. However coercivity is in agreement as enhancement of anisotropic constant and is highest for 0.75 mol Nd concentration in Barium Hexaferrite. The coercivity of the order of (5234.4) Gauss is in agreement with research groups [33,34]. This shows the prepared materials is magnetically hard at nanoscale. But the degree of hardness decreases by substitution of  $\text{Nd}^{3+}$  ions. In this present work local strain produces disorderness. More ever spin-orbit coupling (3d-4f) may be responsible for change in super exchange interaction.

### 3.3. Magnetization and temperature(M-T) measurements

Curie point measurement has been done for sample  $(\text{BaFe}_{12-x}\text{Nd}_x\text{O}_{19})$  for  $X = 0.00, 0.25, 0.50, 0.75$  and  $X = 1.00$  using vibrating sample magnetometer and are shown in Fig. 8. It helps us to idealize the transition of a magnetic materials. The temperature dependent magnetization measurement were carried out from range 45–550°C. The curie point is observed to be shifted to a lower temperature value (429 °C) from 446 °C with Neodymium substitution. The decrease in the  $\text{Fe}^{3+}$  ions may be one reason guided by decrement in exchange interactions between iron ions. Such observation with the Bigger ionic radii dopant has been also reported by research groups [36,39]. All the prepared materials shows pure form with good magnetization (43.11 emu/g–56.90 emu/g), retentivity (21.41 emu/g–29.02 emu/g) at room temperature, which may be useful in magnetic storage data applications. However Curie temperature was shifted to 429 °C from 446 °C for pure phase, which suggests that it favours low energy loss in the prepared material. So it may be fruitful in high density magnetic recording purpose. Some research group also reported low temperature synthesis rare earth substituted ferrite for high frequency applications and others sector [40].

## 4. Conclusions

The Neodymium substituted barium hexaferrite nanomaterials  $((\text{BaFe}_{12-x}\text{Nd}_x\text{O}_{19}))$  for  $(x = 0.0 \text{ to } 1.0)$  has been synthesized using low cost citrate precursor based sol gel method in low temperature range. All nanomaterials synthesized possess hexagonal in nature belonging to space group P63/mmc. There is an increment in the edge parameters(c) and lattice volume steadily because of increment in the molar concentration of Nd in barium hexaferrite lattice at iron site. But there is asystematic decrement in crystallite size and lattice strain with the increasing concentration of Neodymium. Saturation magnetization values are highest for 0.25 mol doped Barium hexaferrite and of the order of 58.24 emu/g. Whereas maximum coercivity values are found for 0.75 mol Nd doped barium hexaferrite. The maximum coercivity value is (5234.4) Gauss. It is observed that magnetization and anisotropy values are maximum for 0.25 mol Nd doped Barium lattice but both these magnetic values decreases for higher concentration of Nd in a similar fashion with minimum values for 1 mol Nd concentration. The curie point is observed to be shifted to a lower temperature value (429 °C) from 446 °C with Neodymium substitution. The decrease in the  $\text{Fe}^{3+}$  ions may be one reason guided by decrement in exchange interactions between iron ions.

## Declaration of Competing Interest

The authors declare that they have no known competing financial interests or personal relationships that could have appeared to influence the work reported in this paper.

## Acknowledgements

Author Harendra Kr Satyapal is thankful to UGC, India, for availing RGNF Fellowship as financial with beneficiary Id-BININ00419091. Authors are thankful to Department of Education, Govt. of Bihar Aryabhata Knowledge University, Patna, which has been very supportive in establishment and functioning of Aryabhata Center for Nanoscience & Nanotechnology, AKU, Patna, Bihar, India. Author Rakesh Kr Singh also thankful for partial financial support to TEQIP-3 of AKU, Patna.

## References

- [1] A.V. Rane, G.J. Phatak, S.K. Date, IEEE Trans Magn. 49 (2013) 5048.
- [2] A. Kumar, V. Agarwala, D. Singh, Prog. Electromagn. Res. 29 (2013) 223.
- [3] A. Arora, S.B. Narang, K. Pubby, J. Magn. Magn. Mater. 423 (2017) 441.
- [4] W. Widanarto, F. Amirudin, S.K. Ghoshal, M. Effendi, W.T. Cahyanto, J. Magn. Magn. Mater. 426 (2017) 483.
- [5] S. Bierlich, F. Gellersen, A. Jacob, J. T€opfer, Mater. Res. Bull. 86 (2017) 19.
- [6] M.A. Ahmed, N. Okasha, R.M. Kersh, Physica B 405 (2010) 3223.
- [7] V. Adelskold, Avk Miner.A 12 (1) (1938).
- [8] C.M. Fang, F. Kools, R. Metselaar, G. de With, R.A. de Groot, J. Phys. Condens. Matter. 15 (2003) 6229.
- [9] M. Feng, B. Shao, J. Wu, X. Zuo, J. Appl. Phys. 113 (2013) 17D909.
- [10] L.S.I. Liyanage, S. Kim, Y.-K. Hong, J.-H. Park, S.C. Erwin, S.-G. Kim, J. Magn. Magn. Mater. 348 (2013) 75.
- [11] C.H. Ri, L. Li, Y. Qi, J. Magn. Magn. Mater. 324 (2012) 1498.
- [12] Y. Wu, Y. Huang, L. Niu, Y. Zhang, Y. Li, X. Wang, J. Magn. Magn. Mater. 324 (2012) 616.
- [13] D.M. Hemeda, A. Al-Sharif, O.M. Hemeda, J. Magn. Magn. Mater. 315 (2007) L1.
- [14] M.J. Iqbal, M.N. Ashiq, I.H. Gul, J. Magn. Magn. Mater. 322 (2010) 1720.
- [15] D. Ionescu, M. Kovaci, IOP Conf. Ser. Mater. Sci. Eng. 95 (2015) 012030.
- [16] M.A. Iqbal, W. Tahir, G. MurtazaRai, N.A. Noor, S. Ali, K.T. Kubra, Ceram. Int. 38 (2012) 3757.
- [17] S.M. Attia, A.M. Abo El Ata, D. El Kony, J. Magn. Magn. Mater. 270 (2004) 142.
- [18] H. Yanbing, S. Jian, S. Lina, T. Quan, L. Qin, J. Hongxiao, J. Dingfeng, B. Hong, G. Hongliang, W. Xinqing, J. Alloys Compd. 486 (2009) 348.
- [19] S. Singhal, A.N. Garg, K. Chandra, J. Magn. Magn. Mater. 285 (2005) 193.
- [20] H.J. Kown, J.Y. Shin, J.H. Oh, J. Appl. Phys. 75 (1994) 6109.
- [21] P. Wartewig, M.K. Krause, P. Esquinazi, S. Rosler, R. Sonntag, J. Magn. Magn. Mater. 192 (1999) 83.
- [22] R. Carey, J. Appl. Phys. 75 (1991) 6789.
- [23] X. Battle, J. Appl. Phys. 70 (1991) 1614.
- [24] X. Battle, J. Appl. Phys. 74 (1993) 3333.
- [25] Sung Yong An, In-Bo Shim, Chul Sung Kim, J. Appl. Phys. 91 (2002) 8465.
- [26] S.V. Trukhanov, A.V. Trukhanov, V.G. Kostishyn, L.V. Panina, V.A. Turchenko, D. I. Tishkevich, E.L. Trukhanova, V.V. Oleynik, O.S. Yakovenko, D.A. Vinnik, L.Yu. Matzui, J. Magn. Magn. Mater. 442 (2017) 300.
- [27] A.V. Trukhanov, V.O. Turchenko, I.A. Bobrikov, S.V. Trukhanov, I.S. Kazakevich, A.M. Balagurov, J. Magn. Magn. Mater. 393 (2015) 253–259.
- [28] Vaishali V. Soman, V.M. Nanoti, D.K. Kulkarni, Ceram. Int. 39 (2013) 5713–5723.
- [29] Vinod N. Dhage, M.L. Mane, A.P. Keche, C.T. Birajdar, K.M. Jadhav, Physica B 406 (2011) 789–793.
- [30] P. Bahera, S. Ravi, J. Supercond. Nov. Magn. 30 (2016) 1453.
- [31] S. Kumar, S. Supriya, L.K. Pradhan, Manoranjan Kar, J. Mater. Sci. Mater. Electron. 28 (2017) 16679.
- [32] Xu. Ping, Xijiang Han, Maoju Wang, J. Phys. Chem. C 111 (2007) 5866–5870.
- [33] R. Kumar, R.K. Singh, M.K. Zope, M. Kar, Mater. Sci. Eng. B 220 (2017) 73.
- [34] S. Kumar, S. Supriya, R. Pandey, L.K. Pradhan, R.K. Singh, M. Kar, J. Magn. Magn. Mater. 458 (2018) 30–38.
- [35] R. Topkaya, J. Alloy. Compd. 725 (2017) 1230.
- [36] R. Grossinger, Phys. Status Solidi A J. Magn. Magn. Mater. 28 (1982) 137.
- [37] V. Anbarasu, T. Karthik, K.S. Kumar, P.M.M. Gazzali, A. Manigandan, J. Mater. Sci. Mater. Electron. 24 (2013) 916.
- [38] S. Mahadevan, C. Pahwa, S.B. Narang, P. Sharma, J. Magn. Magn. Mater. 441 (2017) 465.
- [39] B. Boyanov, J. Univ. Chem. Tech. Metall. 41 (1) (2006) 61–64.
- [40] Rakesh Kr Singh, Jyoti Shah, R.K. Kotnala, Mater. Sci. Eng. B. 210 (2016) 64–69.